phenomenon that is highly dependent on the particular geometric configuration; modified delta wings appear to exhibit similar behavior as unmodified wings and they are dominated by either vortex asymmetry or vortex burst. Extended winglets with a winglet-length to chord-length ratio of 0.43 appear to increase the envelope of operation of the wing substantially in the small apex half-angle region where wing rock occurs. No conclusions can yet be drawn on the relative increase of the drag coefficient over the baseline configuration; however, any adverse effects in the drag coefficient are likely to be outweighed by the benefits of enhanced lift characteristics. These preliminary results indicate that passive control of wing rock may be an effective method for increasing and enhancing the stability of delta wings at high angles of attack.

Acknowledgments

This research was supported by a Presidential Young Investigator Grant from the National Science Foundation to Costas Synolakis. We are grateful to L. E. Ericsson for many interesting suggestions.

References

[1]Gad-El-Gak, M., and Ho, C.-M., "The Pitching Delta Wing," *AIAA Journal*, Vol. 23, No. 11, 1985, pp. 1660–1665.

[2]Ericsson, L. E., and Reding, J. P., "Unsteady Aerodynamics of Slender Delta Wings at Large Angles of Attack," *Journal of Aircraft*, Vol. 12, No. 9, 1975, pp. 721–729.

[3]Polhamus, E. C., "Predictions of Vortex Lift Characteristics by a Leading Edge Suction Analogy," *Journal of Aircraft*, Vol. 8, No. 4, 1971, pp. 193–199.

[4]Nguyen, L. T., Ericsson, L. E., Yip, L. P., and Chambers, J. R., "Self-Induced Wing-Rock on Slender Delta Wings," AIAA Paper 81-1883, Aug. 1981.

[5]Ericsson, L. E., "The Fluid Mechanics of Slender Wing Rock," *Journal of Aircraft*, Vol. 21, No. 5, 1984, pp. 323–328.

[6]Levin, D., and Katz, J., "Dynamic Load Measurements of Delta Wings Undergoing Self-Induced Roll Oscillations," *Journal of Aircraft*, Vol. 21, No. 9, 1984, pp. 30–36.

[7]Ericsson, L. E., "Analytic Predictions of the Maximum Amplitude of Slender Wing Rock," *Journal of Aircraft*, Vol. 26, No. 1, 1989, pp. 35–39.

[8]Ericsson, L. E., "Slender Wing-Rock Revisited," AIAA Paper 91-0417, Jan. 1991.

[9]Katz, J., and Levin, D., "Self-Induced Roll Oscillations Measured on a Delta Wing/Canard Configuration," *Journal of Aircraft*, Vol. 23, No. 11, 1989, pp. 815–819.

Computational Method for Matching Aerodynamic Experimental Data with Theoretical Influence Matrices

Claudio Ponzi*
Alenia, Rome, Italy

Nomenclature

$[A]$ = aerodynamic influence matrix
AR = wing aspect ratio
a_{ij} = generic element of $[A]$
I_i = performance index, defined for each aerodynamic center point
L = number of matched coefficients per aerodynamic center point
N = order of $[A]$
S_1 = set of aerodynamic coefficients which must fit experimental results
S_2 = set of aerodynamic coefficients assumed not to need any correction
s = wing semispan
t = wing aspect ratio
$(\boldsymbol{\alpha})$ = vector of panel angles of attack on control points
$(\Delta \boldsymbol{c}_p)$ = differential pressure coefficient vector across the aerodynamic panel
Λ = wing sweep
τ = theoretical grid point location on the wing semispan axis

Received Aug. 31, 1991; revision received Dec. 30, 1991; accepted for publication Jan. 2, 1992.

*Aerospace Engineer, Corporate Research and Development Department.

Introduction

AERODYNAMIC influence matrices relate local aerodynamic pressure coefficients at collocated grid points and local angles of attack at some other (different) grid points. They are obtained, e.g., through the so-called panel methods. Some examples are the HISSS[1] Code and the "vortex lattice method."[2,3] Panel methods are suitable for studying both subsonic and supersonic flows in steady and unsteady conditions. The latter case leads to frequency-domain airloads, i.e., angles of attack and aerodynamic matrices that are frequency-dependent quantities. All of the following developments are valid within this unsteady flow frame as well.

Panel methods compare well with experimental data provided that the flow conditions are in good agreement with the implicit assumptions of the linearized potential flow model. The purpose of this work is to analyze how experimental pressure data can be used to improve the agreement between theory and experiment, thereby enhancing the use of numerical results.

Solution Procedure

In this article, the term "similar aerodynamic grid" means 1) similar wing planform (same aspect ratio, same sweep angle, same thickness percentage together with equal Mach number); and 2) equal distribution of aerodynamic center points and control points at defined chordwise and spanwise percentage locations. The case in which the theoretical and experimental aerodynamic grids are similar is examined first.

In a linear aerodynamic theory, the aerodynamic influence matrix relates the differential pressure coefficient vector $(\Delta \boldsymbol{c}_p)$ and the vector of panel angles of attack $(\boldsymbol{\alpha})$ in the following form:

$$(\Delta \boldsymbol{c}_p) = [A](\boldsymbol{\alpha}) \tag{1}$$

Expanding Eq. (1) one obtains

$$\Delta \boldsymbol{c}_{pi} = \sum_{j=1}^{N} a_{ij} \boldsymbol{\alpha}_j \tag{2}$$

One can split Eq. (2) into two contributions, according to the fact the theoretical matrix $[A]$ is supposed to fit a set of experimental results

$$\Delta \boldsymbol{c}_{pi} = \sum_{n \in S_1} a_{in} \boldsymbol{\alpha}_n + \sum_{m \in S_2} a_{im} \boldsymbol{\alpha}_m \tag{3}$$

where S_1 has to be interpreted as the set of coefficients which must fit experimental results, while S_2 represents the set of the remaining theoretical coefficients. Assuming the S_2 coefficients to be known, they can be put on the right side of Eq. (3) together with $\Delta \boldsymbol{c}_{pi}$. The number of elements of S_1 (respectively S_2) is L (respectively $N - L$) and the upper bound for L is the number of linearly independent aerodynamic settings of the aircraft (equal to the single movable surface unit deflections and the global unit angle of attack). When solving Eq. (3), a maximum of L unknown influence coefficients can be taken into account for each row i of the system:

one solves separately for each i and thus gets N solutions of L equations. This is equivalent to rewriting L times Eq. (3) in the form Eq. (4) for each set of performed measurements Δc_{pi} and solving for the L coefficients a_{in}. The new system is

$$\begin{cases} \sum_{n=1}^{L} a_{in}\alpha_n^{(1)} = \Delta c_{pi}^{(1)} - \sum_{m=L+1}^{N} a_{im}\alpha_m^{(1)} \\ \sum_{n=1}^{L} a_{in}\alpha_n^{(2)} = \Delta c_{pi}^{(2)} - \sum_{m=L+1}^{N} a_{im}\alpha_m^{(2)} \\ \vdots \\ \sum_{n=1}^{L} a_{in}\alpha_n^{(L)} = \Delta c_{pi}^{(L)} - \sum_{m=L+1}^{N} a_{im}\alpha_m^{(L)} \end{cases} \tag{4}$$

When dealing with large models (high N), selecting the a_{in} may not be evident. A criterion for choosing the L unknowns can be, e.g., to minimize the performance index defined as

$$I_i = \sum_{j=1}^{L} [(a_{ij}^{\text{exp}} - a_{ij}^{\text{th}})/a_{ij}^{\text{th}}]^2 \tag{5}$$

where a_{ij}^{exp} represents the experimentally-matched aerodynamic coefficient and a_{ij}^{th} the theoretical coefficient. The summation can extend to L if one needs to match L aerodynamic coefficients. It can however be extended to L^* with ($L^* < L$). The reason for selecting such an index is justified by the fact that the theoretical aerodynamic matrix $[A]$ is assumed to be globally "good" and therefore only minimum relative changes in $[A]$ should be required.[4]

When assumptions 1) and 2) are not fulfilled, one cannot directly use these results. The case where assumption 1) is even partially violated is not taken into account here. Violation of hypothesis 2) is frequently encountered: in this case, experimental pressure coefficient data have to be transferred from the experimental grid onto the theoretical grid. This can be accomplished through the so-called beaming operation.[5] Once this operation is performed, one can use all of the previous analytical developments.

Assuming that both assumptions 1) and 2) are fulfilled, experimental pressure coefficients may be affected by the flexibility of the model: this fact can be almost completely avoided in wind-tunnel measurements by using rigid models; some conceptual provisions, however, have to be made when considering aeroelastic models in wind tunnels and flight testing experiments. In these cases, sensors are able to measure elastified quantities such as angles of attack and pressure coefficients. In a linear aeroelastic theory, which is commonly accepted by aeroelasticians, elastic local pressure coefficients are linearly related to elastic local angles of attack by means of the $[A]$ matrix in the form represented by Eq. (1), which therefore, appears to be in perfect accordance with both rigid and elastic aerodynamic measurements.

Numerical Simulation

In order to prove the efficiency of the method, the relationships developed in the last sections are used here on a simple example. Here a wing with an aspect ratio of 5, a constant sweep angle of 45 deg, a taper ratio of 1 and an uncambered section are considered. The flowfield is considered to be steady and to be symmetric with respect to the $y = 0$ plane, i.e., there is no yaw. The wing is discretized into a 4 × 1 aerodynamic vortex lattice. A sketch of the wing is represented in Fig. 1. The evaluation of the $[A]$ matrix is performed analytically and reads

$$\begin{cases} \Delta c_{p1} = 2.64133\alpha_1 + 0.55599\alpha_2 + 0.17172\alpha_3 + 0.06187\alpha_4 \\ \Delta c_{p2} = 0.99171\alpha_1 + 2.10180\alpha_2 + 0.40397\alpha_3 + 0.11320\alpha_4 \\ \Delta c_{p3} = 0.54344\alpha_1 + 0.71843\alpha_2 + 1.99623\alpha_3 + 0.34038\alpha_4 \\ \Delta c_{p4} = 0.30923\alpha_1 + 0.35451\alpha_2 + 0.60457\alpha_3 + 1.86853\alpha_4 \end{cases} \tag{6}$$

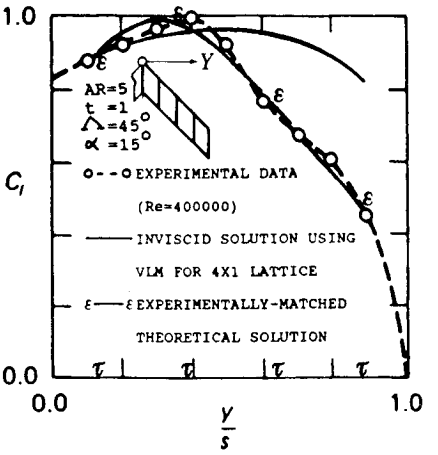

Fig. 1 Comparison of the theoretical, the experimental (wind tunnel) and the experimentally matched theoretical spanwise lift distribution for a wing with $AR = 5$, $\Lambda = 45$ deg, $t = 1$ and an uncambered section in incompressible flow at $\alpha = 15$ deg.

Table 1 Absolute and relative variation in the aerodynamic influence coefficients after experimental matching

AIJ	Theoretical coefficient	Matched coefficient	Relative variation
A11	2.64133	2.55442	−0.03290
A12	0.55599	0.46908	−0.15632
A13	0.17172	0.08481	−0.50611
A14	0.06187	−0.02504	−1.40472
A21	0.99171	1.13163	0.14109
A22	2.10180	2.24172	0.06657
A23	0.40397	0.54383	0.34621
A24	0.11320	0.25312	1.23604
A31	0.54344	−0.26964	−1.49617
A32	0.71843	−0.09465	−1.13175
A33	1.99623	1.18315	−0.40731
A34	0.34038	−0.47270	−2.38874
A41	0.30923	−0.95421	−4.08576
A42	0.35451	−0.90893	−3.56391
A43	0.60457	−0.65887	−2.08982
A44	1.86853	0.60509	−0.67617

Fig. 1 also shows the comparison of the theoretical, the experimental (wind tunnel) and the experimentally-matched theoretical spanwise lift distribution of the wing obtained for a uniform angle of attack equal to 15 deg. The plain solid curve represents theoretical results before experimental matching while the ε solid curve represents theoretical results after matching. The dotted-dashed curve represents experimental measurements. The indications τ on the semispan axis correspond to the theoretical grid point locations. Since there is only one available experimental data set, at most one aerodynamic coefficient can be corrected per $[A]$ matrix row. Thus, by applying Eq. (4), one can compute the relative variation for each aerodynamic coefficient after experimental matching. Data are reported in Table 1. The performance index defined in Eq. (5) is here equal to the square of the "relative variation," as reported in the aforementioned table.

Some comments can be made at this point:

1) The aerodynamic matrix was matched using one single set of measured pressure coefficients. This improvement has lead to a final identity of local pressure coefficients on the aerodynamic grid (see the dotted-dashed curve and the ε curve of Fig. 1).

2) The criterion for choosing which coefficient should be matched has proved to be efficient and to respect wing geometry: the coefficient which minimizes the index I_i of Eq. (5) is equal to the corresponding diagonal term of the $[A]$ matrix. The largest index I_i is the one relative to the outer-wing panel: this is an obvious result since the largest discrepancies between theory and experiment occur at wing tip.

3) Therefore, the best-match aerodynamic influence matrix which ensures that experimental data be exactly fit is such that

$$\begin{cases} \Delta c_{p1} = 2.55442\alpha_1 + 0.55599\alpha_2 + 0.17172\alpha_3 + 0.06187\alpha_4 \\ \Delta c_{p2} = 0.99171\alpha_1 + 2.24172\alpha_2 + 0.40397\alpha_3 + 0.11320\alpha_4 \\ \Delta c_{p3} = 0.54344\alpha_1 + 0.71843\alpha_2 + 1.18315\alpha_3 + 0.34038\alpha_4 \\ \Delta c_{p4} = 0.30923\alpha_1 + 0.35451\alpha_2 + 0.60457\alpha_3 + 0.60509\alpha_4 \end{cases} \quad (7)$$

Concluding Remarks

A procedure has been developed which finds minimum changes in an analytical aerodynamic influence matrix to make it exactly agree with a set of measured pressure coefficients. It is suitable for application to large matrices where the number of linearly independent sets of available pressure coefficient data is smaller than the total number of panels of the aerodynamic discretization. Provisions for overcoming a nonsimilarity between the experimental and the theoretical aerodynamic grid, as well as aeroelastic effects on the experimental model are straightforward.

References

[1]Fornasier, L., and D'Espiney, P., "Prediction of Stability Derivatives for Missiles Using the HISSS Panel Code," AGARD-CP 451, March 1989.

[2]Woodward, F. A., "An Improved Method for the Aerodynamic Analysis of Wing-Body-Tail Configurations in Subsonic and Supersonic Flow," NASA CR-2228, 1973.

[3]Bertin, J. J., and Smith, M. L., "*Aerodynamics for Engineers*," Prentice Hall, Englewood Cliffs, NJ, 1979, pp. 187–207.

[4]Berman, A., and Nagy, E. J., "Improvement of a Large Analytical Model Using Test Data," *AIAA Journal*, Vol. 21, No. 8, 1983, pp. 1168–1173.

[5]"FASTOP: An Automated Procedure for Flutter and Strength Analysis and Optimization of Aerospace Vehicles," Program User's Manual, Vol. II, Air Force Flight Dynamics Lab., Wright-Patterson AFB, OH, Dec. 1975, pp. 62–72.

Computational Flowfields for Static Testing of Powered Hypersonic Aftbody Models

Lawrence D. Huebner*
NASA Langley Research Center, Hampton, Virginia 23665

Introduction

HYPERSONIC air-breathing vehicles, such as the national aero-space plane (NASP), utilize a supersonic combustion ramjet (scramjet) propulsion system. The location of this scramjet on the underside of the airframe, and the shaping of the forebody and aftbody are prime concerns of propulsion/airframe integration (PAI) to provide optimum aero-propulsive performance. The forebody acts as a precompression region for the inlet flow where the objective is to obtain a high-quality compressed flow to the scramjet inlet while maintaining low-forebody drag. The aftbody, in part, serves as the external scramjet nozzle expansion for the exhaust gases and provides significant force and moment components for the entire vehicle. Consequently, efficient PAI is very important in the design of hypersonic, airbreathing vehicles like the NASP.[1]

PAI is an important facet in the aerodynamic analysis and testing of such NASP-like hypersonic, air-breathing vehicles under simulated powered conditions. Ground-based testing of powered hypersonic, air-breathing configurations is both difficult and expensive due to the high temperatures and pressures necessary to sustain the hydrogen/air combustion proess.[2] Also, size limitations of ground-based facilities preclude duplication of scramjet operation because the combustion process is not geometrically scalable.[2] Furthermore, numerical modeling of the combustion process is expensive, being feasible only with the most powerful supercomputers. In order to obtain powered data and avoid these problems, an experimental technique was developed to simulate the hydrogen/air scramjet exhaust, whereby the inlet is faired over and a simulant gas is routed into a plenum in the model. The simulant gas passes through a combustor nozzle designed for inviscid similitude of the actual combustion process at the combustor exit, and then expands into the aftbody flowfield. The models employing this technique can either be fully metric, utilizing a flow-through balance, have metric and nonmetric parts, or be highly instrumented for surface pressure integration. In either of the last two techniques, it is possible to isolate the aftbody nozzle during powered testing to determine the component force and moment contributions.

To date, powered tests have been performed in hypersonic wind tunnels to provide some freestream similitude with typical flight conditions. However, it is uncertain if the hypersonic (dynamic) environment is truly required for testing powered aftbodies. It has been shown that, at typical values of static nozzle pressure ratio (SNPR, the ratio of the static pressure at the combustor exit to the freestream static pressure), differences in aftbody pressure distributions are insignificant as the freestream Mach number is increased from 4.0 to 14.0 at constant Reynolds number.[3] This then leads to the possibility of an alternate form of powered testing. If an appropriate simulation parameter (like SNPR) can be matched by reducing the pressure of the test section to the local freestream pressure that occurs in the hypersonic flowfield, powered aftbody testing in a static environment may be possible. This technique would allow the model to be much simpler (no realistic forebody required) with a significant decrease in the fabrication and testing expenses. This note presents the method and results of a two-dimensional computational study aimed at assessing the feasibility of conducting static tests to determine the performance of hypersonic, air-breathing aftbody models.

Computational Method

The computational fluid dynamics (CFD) code applied to the configurations of interest in this study is the general aerodynamic simulation program (GASP).[4,5] GASP solves the integral form of the governing equations, including the full Reynolds-averaged Navier-Stokes equations, the thin-layer Navier-Stokes (TLNS) equations, the parabolized Navier-Stokes (PNS) equations, and the Euler equations. The discretized equations may be solved by space-marching or global-iteration, and both explicit multistage Runge-Kutta and implicit time integration schemes are included. The code allows highly flexible coupling of multiple grid zones, each of which may be solved independently or simultaneously. Grid generation for GASP is simplified due to the zonal algorithm, but grid point connectivity is required along the zonal interface boundaries. The

Presented as Paper 91-1709 at the AIAA 22nd Fluid Dynamics, Plasma Dynamics, and Lasers Conference, Honolulu, HI, June 24–26, 1991; received Nov. 30, 1991; revision received Jan. 9, 1992; accepted for publication Jan. 9, 1992.

*Aerospace Engineer, Hypersonics Group Leader, Supersonic/Aerodynamics Branch, Applied Aerodynamics Division, M/S 413. Senior Member AIAA.